Taking for example $h = 25$ nm, $d = 50$ nm, $Q = 83$, and $\Delta T = 100$ K, we find for polystyrene and air (with $\kappa_0 = 0.034$ J $(\mathrm{m\,s\,K})^{-1}$ and $\kappa_p = 0.16$ J $(\mathrm{m\,s\,K})^{-1}$) $J_q \approx 100$ W mm^{-2}. Using these values, Equation 3 predicts $\lambda \approx 100$ nm.

Finally, we note the advantage of a positive replication technique over imprint lithography. The substantially reduced physical contact between the film and the master significantly decreases the effective adhesion between the master and the substrate. This facilitates the release of the master and reduces replication problems stemming from polymeric material that remains on the master after its release. The technique could be easily incorporated into existing fabrication lines and does not need any specialized equipment nor chemicals. Furthermore, a combination of such a thermomechanical instability with electrostatic forces[8] is a promising prospect for a simple, low-cost lithographic technique for the replication of sub-micrometer patterns.

Experimental

The polymer used was polystyrene (PS) with an averaged molecular weight of 108 kg mol^{-1} and a polydispersity of 1.03, purchased from Polymer Standards Service, Mainz and used as obtained. Highly polished silicon wafers were donated to us by Wacker Siltronic, Burghausen. Structured master wafers (by electron-beam lithography) were purchased from x'lith extreme lithography, Illerrieden. As received, all silicon wafers were covered with a native (≈ 2 nm thick) oxide layer. The silicon wafers were cleaned by a jet of carbon dioxide crystals ("snowjet" [22]). The structured master wafer was rendered apolar by deposition of a self-assembled alkane monolayer from solution [23] to minimize its adhesion to the polymer. Au was evaporated on the back side of all silicon wafers, improving the thermal contact and facilitating the short-circuiting of the two plates. Thin polymer films were prepared by spin-coating from analytic grade toluene onto the planar Si substrates. Typical polymer concentrations were 3 wt.-% and rotation speeds were ≈ 4000 rpm, resulting in film thicknesses h of around 100 nm. A topographically structured master wafer was mounted facing the polymer film, leaving an air gap. A schematic representation of the experimental set-up is shown in Figure 1. The plate spacing d was controlled by silicon dioxide spacers (dotted columns in Fig. 1), ranging from 100 to 600 nm. To eliminate the build up of electrostatic charges, both substrates were grounded. One side of the assembly was heated to a temperature T_1 by placing it onto a hot plate, while the other plate was cooled by bringing it into contact with a copper block set to a temperature T_2, which was temperature controlled by perfusion with water. Both temperatures were measured by small thermocouples (PT100) that were embedded into the copper blocks close to the Si wafers. Good thermal contact was ensured by thermal conducting paste. This established a temperature difference $\Delta T = T_1 - T_2$ of typically 10–50 K across the film–air double layer. Both temperatures were kept constant to within 1 K, above the glass transition temperature of the polymer to ensure the liquid state. Together with the small plate spacing this generates large temperature gradients on the order of 10^8 K m^{-1}. While pattern replication is typically completed after less than 1 h (see Eq. 4), we heated the samples over night to assure equilibration. Subsequently, the assembly was rapidly cooled to room temperature (below the glass transition temperature of the polymer). This quench freezes in the topographic structures of the polymer film, which can subsequently be conveniently analyzed or further processed at room temperature. The upper plate was mechanically removed, and the polymer films were characterized by optical and atomic force microscopy.

Received: September 4, 2002
Final version: November 12, 2002

[1] K. Ziemelis, *Nature* **2000**, *406*, 1021.
[2] R. Piner, J. Zhu, F. Xu, S. Hong, C. Mirkin, *Science* **1999**, *283*, 661.
[3] Y. Xia, J. A. Rogers, K. E. Paul, G. M. Whitesides, *Chem. Rev.* **1999**, *99*, 1823.
[4] S. Y. Chou, P. R. Krauss, *Science* **1996**, *272*, 85.
[5] S. Y. Chou, C. Keimel, J. Gu, *Nature* **2002**, *417*, 835.
[6] H. Schift, C. David, M. Gabriel, J. Gobrecht, L. Heyderman, W. Kaiser, S. Köppel, L. Scandella, *Microelectron. Eng.* **2000**, *53*, 171.
[7] M. Böltau, S. Walheim, J. Mlynek, G. Krausch, U. Steiner, *Nature* **1998**, *391*, 877.
[8] E. Schäffer, T. Thurn-Albrecht, T. P. Russell, U. Steiner, *Nature* **2000**, *403*, 874.
[9] Lord Rayleigh, *Proc. London Math. Soc.* **1878**, *10*, 4.
[10] A. Vrij, *Discuss. Faraday Soc.* **1966**, *42*, 23.
[11] F. Brochard-Wyart, J. Daillant, *Can. J. Phys.* **1990**, *68*, 1084.
[12] G. Reiter, *Phys. Rev. Lett.* **1992**, *68*, 75.
[13] R. Seemann, S. Herminghaus, K. Jacobs, *J. Phys.: Condens. Matter* **2001**, *13*, 4925.
[14] W. Mönch, S. Herminghaus, *Europhys. Lett.* **2001**, *52*, 525.
[15] S. Herminghaus, *Phys. Rev. Lett.* **1999**, *83*, 2359.
[16] S. Chou, L. Zhuang, L. Guo, *Appl. Phys. Lett.* **1999**, *75*, 1004.
[17] E. Schäffer, T. Thurn-Albrecht, T. P. Russell, U. Steiner, *Europhys. Lett.* **2001**, *53*, 518.
[18] E. Schäffer, S. Harkema, R. Blossey, U. Steiner, *Europhys. Lett.* **2002**, *60*, 255.
[19] E. Schäffer, S. Harkema, M. Roerdink, R. Blossey, U. Steiner, *Macromolecules* **2003**, *36*, 1645.
[20] E. Schäffer, U. Steiner, *Euro. Phys. J. E* **2002**, *8*, 347.
[21] R. Seemann, S. Herminghaus, K. Jacobs, *Phys. Rev. Lett.* **2001**, *86*, 5534.
[22] R. Sherman, D. Hirt, R. J. Vane, *J. Vac. Sci. Technol.* **1994**, *12*, 1876.
[23] P. Silberzan, L. Léger, D. Ausserré, J. J. Benattar, *Langmuir* **1991**, *7*, 1647.

Chemically Amplified Positive Resists for Two-Photon Three-Dimensional Microfabrication**

By *Tianyue Yu*, *Christopher K. Ober*,* *Stephen M. Kuebler*, *Wenhui Zhou*, *Seth R. Marder*,* and *Joseph W. Perry**

Two-photon excitation (TPE) provides a means for photoactivating chemical and physical processes with high spatial resolution in three dimensions, using a single tightly focused laser beam. TPE has enabled or furthered the development of several important new technologies, including three-dimensional (3D) fluorescence imaging,[1] 3D lithographic microfabrication (3DLM),[2–7] and new approaches to 3D optical data storage.[8,9] In each of these techniques, high spatial resolution is achievable because the two-photon absorption (TPA) probability depends quadratically on the excitation intensity. By tightly focusing an excitation beam, the region of two-photon absorption can be confined at the focus to a volume of the order of the cube of the excitation wavelength ($V \approx \lambda^3$). Any subsequent process, such as fluorescence or a photo-induced chemical reaction, is also localized to this small volume. Two-

[*] Dr. C. K. Ober, Dr. T. Yu
Materials Science and Engineering, Cornell University
Ithaca, NY 14853 (USA)
E-mail: cober@ccmr.cornell.edu
Prof. S. R. Marder, Dr. J. W. Perry, Dr. S. M. Kuebler, Dr. W. Zhou
Department of Chemistry, The University of Arizona
Tucson, AZ 85721 (USA)
E-mail: smarder@u-arizona.edu; jwperry@u-arizona.edu

[**] This research was supported by the National Science Foundation at Cornell University through the Nanobiotechnology Center (ECS-9876771) and at the University of Arizona through the Science and Technology Center for Materials and Devices for Information Technology Research (DMR-010967) and the Chemistry Division (CHE-0107105) and by the AFOSR through the Liquid Crystal MURI (#F49620-97-1-0014). Support from the W. M. Keck Foundation for the purchase of instrumentation used in this research is gratefully acknowledged. The Cornell Nanofabrication Facility is gratefully acknowledged for providing the equipment for initial photolithographic evaluation of the materials.

  0935-9648/03/0603-0517 $ 17.50+.50/0

ADVANCED MATERIALS

photon 3D microfabrication offers a direct route to many micromachined structures that can have applications in micro-optics, microfluidics, microelectro-mechanical systems (MEMS), and optical data storage.[2–9] Two-photon lithography not only allows the fabrication of structures that are difficult to access by conventional single-photon processes, but also possesses greater spatial resolution than other 3D microfabrication techniques as they are currently practiced.[10–13] Recently, highly efficient two-photon absorbing dyes,[14,15] and radical and acid generators have been developed.[16,17] Microfabrication of 3D microstructures has been accomplished by radical polymerization of crosslinkable acrylate resin systems,[6,16] but volume shrinkage and distortion of the solid images formed in such systems can limit its use. As an alternative approach, 3D microstructures can also be fabricated using positive tone solid-state resists, wherein the exposed regions can be removed in a development step. In this paper, we report a chemically amplified positive-tone polymeric system that can be efficiently patterned by two-photon excitation, and in which the unexposed regions undergo little structural distortion during processing.

To develop a chemically amplified resist system for two-photon lithography, random copolymers of tetrahydropyranyl methacrylate (THPMA), methyl methacrylate (MMA) and *tert*-butyl methacrylate (*t*BMA) were designed and synthesized. The general structure of the copolymer is shown in Figure 1. In the presence of acid, a deprotection reaction generates poly(methacrylic acid) after the removal of the THP and *tert*-butyl protecting groups, and converts the non-acidic copolymer to one that can be easily dissolved using aqueous base developer. The polymer is designed such that it is soluble in organic solvents for film casting, and so that the unexposed material is neither dissolved nor swollen by aqueous base developer. Thus the unexposed regions undergo little or no distortion during exposure or development. In the design of the copolymer system we chose MMA to provide strength and optical clarity, while the THPMA and the *t*BMA were chosen to provide the acid catalyzed change in solubility. We recently reported a photoacid generator (PAG), whose structure is shown in Figure 1, that was designed to have a large two-photon cross section and a high quantum yield for acid generation. Positive tone resins for two-photon patterning were prepared that comprised 4 wt.-% PAG and 96 wt.-% THPMA/MMA/*t*BMA copolymer.

Table 1 lists the compositions of a series of random copolymers of THPMA, methyl methacrylate, and *t*BMA with different compositions. The MMA content was fixed at 60 mol-%, while the THPMA and *t*BMA content ranged from 0 to 40 mol-% in the copolymer. It should be noted that THPMA and *t*BMA have very different activation energies for the acid-deprotection reaction, with THPMA being more reactive.[18,19] The copolymer design therefore enables one to tune the rate of acid cleavage.

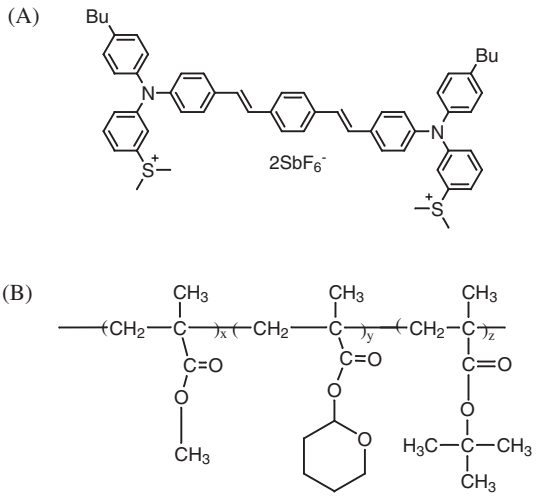

Fig. 1. A) Chemical structure of the two-photon photoacid generator used in this work. B) Generic composition of the photopolymers used in this work.

Unlike 2D lithography, where a contrast curve can be obtained by measuring the film thickness change as a function of exposure dose, in 3D lithography it is rather difficult to measure volumetric resolution in the lithographic process. We employed a qualitative method to compare the lithographic sensitivity of the above polymer systems. Cubic structures, 5 μm on a side, were subjected to different exposure intensities and times in a given film. After post-exposure bake and development steps, the patterned film was imaged using two-photon fluorescence microscopy to obtain a 3D image of the fabricated structure. Figure 2A shows images that illustrate how the exposed region appeared when it was: i) underexposed/underdeveloped, ii) properly exposed/fully developed, and iii) overexposed/overdeveloped. The ratio of the developed volume to the volume exposed (the height of the columns in Fig. 2) was estimated based on the vertical profile of the developed structures. Using this semiquantitative indication of the degree of exposure and/or development, the sensitivities of the copolymers in Table 1 were compared under the same processing conditions (Figs. 2B,C). The PMMA–THPMA (P6) system was found to possess the highest sensitivity, as expected given the low activation energy for cleavage of the THP ester linkage. Figure 2 shows that the threshold of P6 is around 40 μW, as compared to 160 μW for P5 under the same processing conditions.

For copolymer compositions with greater than 16 mol-% of *t*BMA it was found that precipitation of the photoacid genera-

Table 1. Copolymer compositions and molecular weight data.

Copolymer	Monomer feed fractions (PMMA/*t*BMA/THPMA)	Experimental composition (^{1}H NMR)	Molecular weight (M_n)	Polydispersity
P1	60:40:0	57.6:42.4:0.0	46.6K	1.8
P2	60:32:8	57.2:34.7:8.1	18.2K	2.2
P3	60:24:16	58.7:25.7:15.6	22.3K	2.2
P4	60:16:24	57.0:16.8:26.2	20.1K	2.3
P5	60:8:32	56.0:17.0:27.0	19.5K	2.3
P6	60:0:40	62.2:0.0:37.8	19.9K	2.2

  0935-9648/03/0603-0518 $ 17.50+.50/0

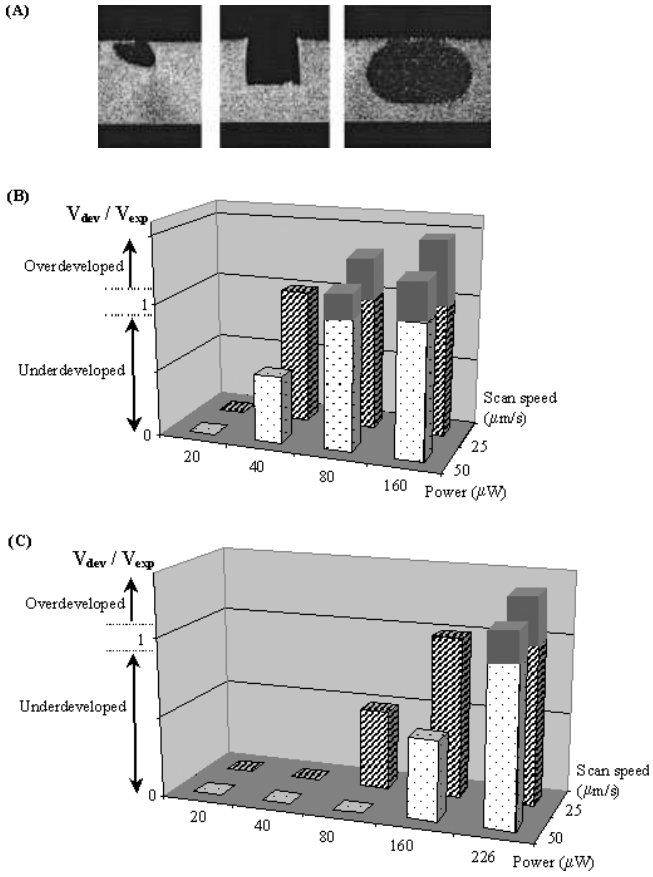

Fig. 2. A) Two-photon fluorescence images illustrating the vertical profile and extent of etching at various stages of development. The bright region is the polymer film containing two-photon acid generator and the dark region is where polymer has been removed. Comparison of two-photon photosensitivities for B) PMMA–THPMA (P6: 60:40), and C) PMMA–THPMA–*t*BMA (P5: 60:32:8). The ratio of the volume developed to the volume exposed (V_{dev}/V_{exp}) is plotted as a function of power for two different stage scan speeds. The films were processed under the same conditions (60 min pre-exposure bake at 90 °C, 1 min post-exposure bake at 120 °C, developed in 0.26 N TMAH for 1 min) except that they were patterned under various exposure conditions (by variation of power and stage scanning speed). The system based on PMMA–THPMA–*t*BMA (60:24:16) showed no development under the above conditions. Systems with higher *t*BMA content had poor optical quality and were not included in the sensitivity comparison.

tor in the polymer matrix occurred and the optical clarity of the film was degraded. This reduced solubility of the photoacid generator may be due to the lower polarity of the *tert*-butylester relative to the other esters. The *tert*-butyl group requires a higher post-exposure bake temperature than the THP group to activate its acid-deprotection reaction. Typically, a post-exposure baking temperature of 130–150 °C is used in conventional thin film lithography when a *tert*-butyl group is employed as the deprotection group, while 70–90 °C is used when a THP group is employed. In films used here for 3D microfabrication, the film thickness is in the range of tens to hundreds of micrometers. It was observed that high post-exposure baking temperatures (> 140 °C) led to foaming of the film, possibly because of the rapid generation of volatile isobutene and 3,4-dihydro-2H-pyran, by-products of the acid deprotection reaction, and the volatization of residual solvent. Deformation of the structures therefore occurred. In this sense, a high activation energy group such as the *tert*-butyl function is less desirable than its low activation energy counterpart in this type of thick film fabrication. For the system of MMA–THPMA copolymer (P6), which does not contain the *t*BMA subunit, a higher post-exposure baking temperature of 120 °C is not only unnecessary but also undesirable because it appears to harden the surface and makes the development difficult. On the other hand, the low activation energy system (P6) may undergo some ester cleavage at room temperature. This type of "dark reaction" can be suppressed by incorporation of base into the resin formula.[20] For these reasons, copolymer P6 was used for two-photon 3D microfabrication studies.

The fidelity of the fabricated structures depends not only on the post-exposure bake process but also on the development process and on the geometry of the structure itself. Clearly, for the solvent developer to remove polymer from the exposed regions of 3D microstructures fabricated in a positive resist system, there must be a continuous pathway of exposed material leading from the structure to the surface. During the development process, the aqueous base solvates polymer chains leading to swelling and ultimately to dissolution. Since the removal of polymer chains from the surface of the exposed region is diffusion-limited process, the extent of development in a given period of time is dependent on the length and aspect ratio of the feature to be developed. To investigate the effect of feature geometry on the extent of development, we fabricated a series of channel type structures with different aspect ratios, which we characterize with an aspect-ratio parameter ARP = (channel length)/(cross-sectional area). A threshold aspect-ratio parameter can be defined as the maximum ARP that, for a given material and set of development conditions, leads to complete removal of the exposed/deprotected volume. For a given material and processing conditions, a larger threshold ARP value for a channel feature indicates that longer and thinner channels can be fabricated.

We designed and fabricated simple buried channels that are connected to cubic or prismatic trenches that are open to the surface (Fig. 3). The progress of the development of the structure was monitored by optical microscopy and was stopped when the two trenches appeared to be fully developed. At this point, the interconnecting channels were not necessarily fully developed. If the development was conducted for a longer period of time, the trenches became overdeveloped and distorted. This could be due to either spontaneous thermal deprotection of, or base attack on, the THP ester groups. These deleterious side reactions impart partial solubility to the unexposed material and place limitations on the shelf life of the films and the duration of the development process.

We have found that the channel-forming ability of the structure depends on the shape of the trench. If the trench is changed from a cubic structure to a prismatic structure, as shown in Figure 3B, the threshold ARP values of the channels increased from ~ 3 to ≥ 5. It was also observed that in the case

  0935-9648/03/0603-0519 $ 17.50+.50/0

ADVANCED MATERIALS

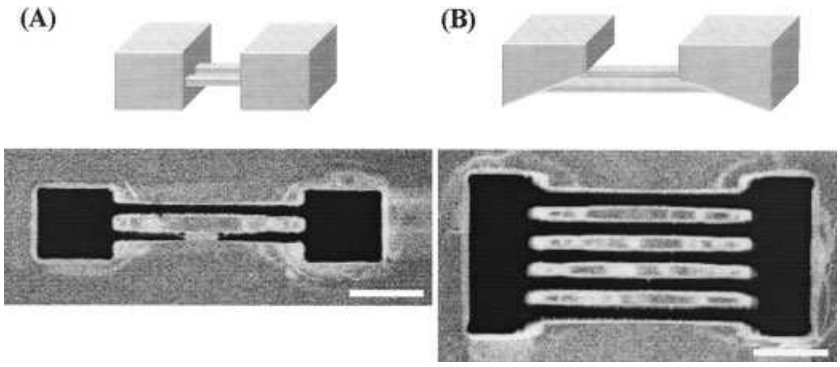

Fig. 3. Top: Illustration of two 3D structures shown A) with cubic trenches and B) with prismatic trenches. Bottom: Two-photon fluorescence images of microchannels, located in a plane 10 μm below the surface. A) Upper channel: 50 μm × 4 μm × 4 μm (ARP = 3.1), fully developed; Bottom channel: 50 μm × 4 μm × 3 μm (ARP = 4.6), not fully developed. B) channels in the modified structure. Channel geometry: 70 μm × 4 μm × 4 μm (ARP = 4.4) all the same size, fully developed. The scale bars correspond to 20 μm.

of the cubic trenches, the channel openings would become partially clogged during development, whereas this was not observed for the case of the prismatic trenches. It is clear that the larger area of the opening and the inclined surface for the prismatic trench can facilitate improved transport of solution into, and polymer chains out of, the channel.

Using this knowledge, we designed and fabricated an optical grating structure comprising a set of twelve parallel channels buried about 10 μm below the surface with connecting reservoirs on both ends, as shown in Figure 4. We have backfilled the structure with a low molar mass liquid crystal mixture suggesting a possible approach to buried switchable grating devices.

The limiting resolution in 3D microlithography is determined by the dimensions of the volume element (voxel) generated by the two-photon exposure. The final size of the voxel depends on the focal spot size, the exposure conditions (laser power and scan speed), and the chemical and physical processes that occur as a result of the photoexcitation and the development processes employed following exposure. Consequently, the smallest achievable voxel will be of the order of the focused spot-size, although the processing conditions and aspects of the photochemistry can result in voxel sizes that are much larger than the focal spot. For the experiments described here, the transverse and longitudinal dimensions (full width at half maximum) of the diffraction-limited focal spot may be estimated under the paraxial approximation[21,22] as $W = 0.27$ μm and $L = 1.0$ μm, respectively (assuming $n_{resin} \approx 1.5$). These dimensions are comparable to that of the smallest polymerized features we have obtained by two-photon-initiated polymerization of an acrylate resin using similar conditions.[23] Inspection of Figures 3 and 4 reveals that the edges of the positive-resist structures are rounded. This most probably results from diffusion of protons during the post-exposure bake step. It should be possible to further improve resist resolution and

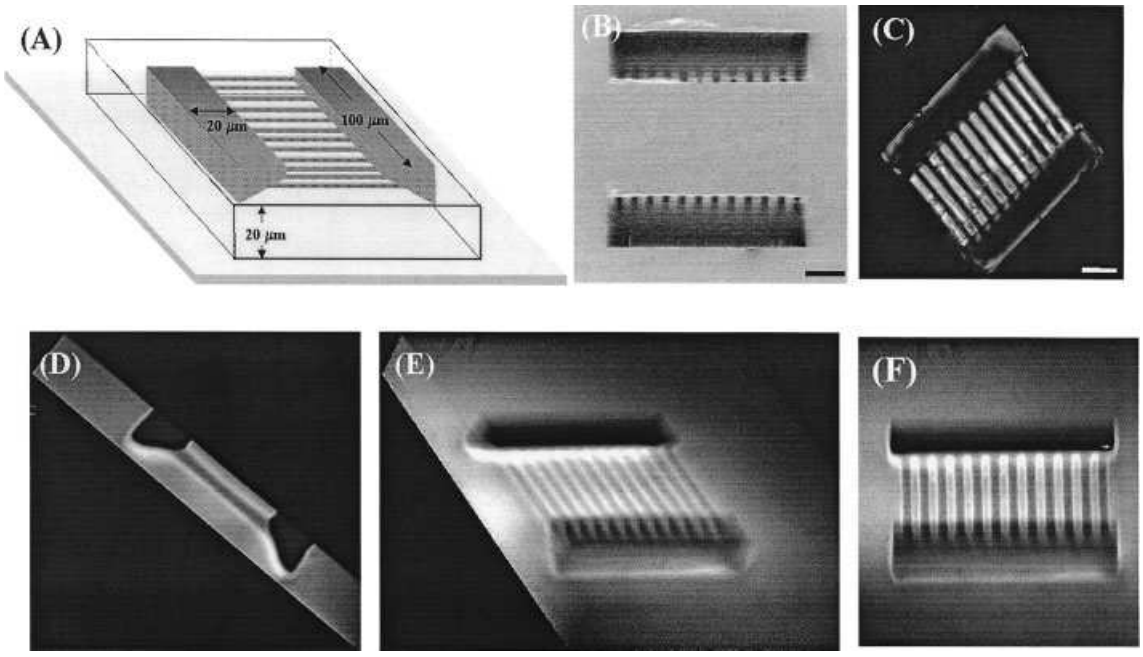

Fig. 4. Illustration of: A) Target structure consisting of two prismatic cavities (width: 100 μm, length: 20 μm, depth: 20 μm), that are connected by twelve channels (length: 50 μm; 4μm × 4 μm cross-section) with a periodicity of 8 μm and lying 10 μm below the surface. B) Scanning electron microscopy (SEM) image of the final structure, viewed normal to the substrate. C) Polarized optical microscope image of the grating structure after filling with E7 liquid crystal. The scalebars in B and C correspond to 20 μm. D–F) 3D reconstructed images of the optical grating structure obtained by using two-photon fluorescence imaging at different depths through the structure. (rotation angles: D) 90° view; E) 45° view; F) 0° view).

  0935-9648/03/0603-0520 $ 17.50+.50/0

overall performance by the addition of small amounts of base to reduce proton diffusion into unexposed regions. We can estimate the width of the etched voxel to be ~1.0 μm. As the width of the voxel is much larger than that of the focal spot, the experimental conditions used to process the resist may not be optimized for achieving the smallest voxel. We are currently exploring other exposure and development conditions and modified resin systems to further improve the resolution in this type of 3D microlithography.

In conclusion, we have developed a chemically-amplified positive resist material and processing conditions that enable the microfabrication of buried 3D structures using two-photon lithography. The ability to selectively remove material in exposed regions allows for efficient creation of small hollow features within a larger solid body. By tailoring the polymer structure, it should be possible to fabricate the 3D structures with selected surface properties. For example, in our material, the pendent chemical groups at the patterned surface are methacrylic acid groups that provide a variety of options for surface functionalization. This feature may be useful for microfluidic devices for biological applications, and makes possible the study of both chemical and geometrical factors for such applications. These results suggest that positive tone two-photon 3D microfabrication may be a valuable route to precision microfluidic and micro-optical devices.

Experimental

The polymers used in this study were synthesized by copolymerization of THPMA, MMA, and *t*BMA [18,19]. The number average molecular weight (M_n) and the polydispersity of the copolymers were determined by gel permeation chromatography (THF, solvent) using polystyrene as the standard. The copolymer compositions were verified by ^{1}H NMR measurements that were carried out in $CDCl_3$ at room temperature with a Varian INOVA-400 spectrometer operating at 400 MHz for protons (Table 1). A two-photon 3D microfabrication resin system was created by blending 4 wt.-% of the two-photon acid generator [17] into the above-synthesized copolymers. 3D microfabrication was carried out using thick polymeric films (~50 μm) prepared by blade casting from γ-butyrolactone (GBL). The films were baked at 90 °C for 1 h under a nitrogen atmosphere. The system for two-photon 3D microfabrication has been described elsewhere [17]. The PAG was excited with ~100 fs pulses at a wavelength of 745 nm. The samples were mounted on a computer-controlled 3D translation stage. The incident beam was focused through an oil-immersion objective with a numerical aperture of 1.4. By scanning the focal point of the laser beam through the film, 2D and 3D patterns were defined. The total exposure dose is determined by the laser power and linear scan speed (dwell time in a voxel) of the stage. After exposure, the film was baked and developed in 0.26 N tetramethyl ammonium hydroxide (TMAH) aqueous solution and monitored by optical microscopy. The 3D microstructures shown in Figures 3 and 4 were fabricated by two-photon-exposure in a 50 μm thick film of PMMA–THPMA (60:40). The patterns were exposed at 745 nm at an average power of 40 μW and a linear scan speed of 50 μm s^{-1}. After exposure, the film was baked for 1 min at 90 °C. The target structure was then obtained by dissolving the exposed resin in aqueous 0.26 N tetramethyl ammonium hydroxide.

Received: August 19, 2002
Final version: December 1, 2002

[1] W. Denk, *Proc. Natl. Acad. Sci. USA* **1994**, *91*, 6629.
[2] W. Denk, J. H. Strickler, W. W. Webb, *Science* **1990**, *248*, 73.
[3] J. H. Strickler, W. W. Webb, *Opt. Lett.* **1991**, *16*, 1780.
[4] J. H. Strickler, W. W. Webb, *Proc. Soc. Photo-Opt. Instrum. Eng.* **1990**, *1398*, 107.
[5] E. S. Wu, J. H. Strickler, W. R. Harrell, W. W. Webb, *Proc. Soc. Photo-Opt. Instrum. Eng.* **1992**, *1674*, 776.
[6] S. Maruo, O. Nakamura, S. Kawata, *Opt. Lett.* **1997**, *22*, 132.
[7] S. Maruo, S. Kawata, *J. Microelectromech. Syst.* **1998**, *7*, 411.
[8] D. A. Parthenopoulos, P. M. Rentzepis, *Science* **1989**, *245*, 843.
[9] H. E. Pudavar, M. P. Joshi, P. N. Prasad, B. A. Reinhardt, *Appl. Phys. Lett.* **1999**, *74*, 1338.
[10] K. Ikuta, K. Hirowatari, T. Ogata, in *Proc. of IEEE Int. Workshop on Micro Electro Mechanical Systems*, IEEE, Piscataway, NJ **1994**, p. 1.
[11] T. Takagi, N. Nakajima, in *Proc. of IEEE Int. Workshop on Micro Electro Mechanical Systems*, IEEE, Piscataway, NJ **1994**, p. 211.
[12] M. Horiyama, H. B. Sun, M. Miwa, S. Matsuo, H. Misawa, *Jpn. J. Appl. Phys.* **1999**, *38*, L212.
[13] S. Maruo, K. Ikuta, *Appl. Phys. Lett.* **2000**, *19*, 2656.
[14] M. Albota, D. Beljonne, J.-L. Brédas, J. E. Ehrlich, J.-Y. Fu, A. A. Heikal, S. E. Hess, T. Kogej, M. D. Levin, S. R. Marder, D. McCord-Maughon, J. W. Perry, H. Röckel, M. Rumi, G. Subramaniam, W. W. Webb, X.-L. Wu, C. Xu, *Science* **1998**, *281*, 1653.
[15] M. Rumi, J. E. Ehrlich, A. A. Heikal, J. W. Perry, S. Barlow, Z. Hu, D. McCord-Maughon, T. C. Parker, H. Röckel, S. Thayumanavan, S. R. Marder, D. Beljonne, J.-L. Brédas, *J. Am. Chem. Soc.* **2000**, *122*, 9500.
[16] B. H. Cumpston, S. P. Ananthavel, S. Barlow, D. L. Dyer, J. E. Ehrlich, L. L. Erskine, A. A. Heikal, S. M. Kuebler, I.-Y. S. Lee, D. McCord-Maughon, J. Qin, H. Röckel, M. Rumi, X. Wu, S. R. Marder, J. W. Perry, *Nature* **1999**, *398*, 51.
[17] W. Zhou, S. M. Kuebler, K. L. Braun, T. Yu, C. K. Ober, J. W. Perry, S. R. Marder, *Science* **2002**, *296*, 1106.
[18] K. Ogino, J. S. Chen, C. K. Ober, *Chem. Mater.* **1998**, *10*, 3833.
[19] S. Yang, J. Wang, K. Ogino, S. Valiyaveettil, C. K. Ober, *Chem. Mater.* **2002**, *12*, 33.
[20] K. Asakawa, T. Ushirogouchi, M. Nakase, *Proc. Soc. Photo-Opt. Instrum. Eng.* **1995**, *438*, 563.
[21] R. H. Webb, *Rep. Prog. Phys.* **2000**, *59*, 427.
[22] M. Born, E. Wolf, *Principles of Optics*, 6th ed., Pergamon, Oxford **1993**.
[23] S. M. Kuebler, M. Rumi, T. Watanabe, K. Braun, B. H. Cumpston, A. A. Heikal, L. L. Erskine, S. Thayumanavan, S. Barlow, S. R. Marder, J. W. Perry, *J. Photopolym. Sci. Technol.* **2001**, *14*, 657.

Novel Oxides for Cycled Hydrogen Production from Methane and Water Using a Temperature Swing

Zhenchuan Kang and *Zhong Lin Wang**

A hydrogen-powered energy system has been proposed as the future basis of a green energy economy. Production, storage, distribution, and application of hydrogen are the main challenges for a hydrogen-based technology.[1] More than 90 % of the hydrogen today is made thermochemically through a process called reforming,[2] in which hydrocarbons are reacted with steam or oxygen at high temperature, typically 800–1700 °C. Besides water electrolysis, research has been carried out to explore other hydrogen-production methods at low energy cost,[3] such as the sunlight powered photoelectrochemical cell.[4] Direct oxidation of methane has been achieved using ceria-supported metal catalysts, such as Pt, Rh, Cu, and Ni.[5,6] Ceria is frequently used because of its high activity for hydrocarbon oxidation and high ionic conductivity.[7]

[*] Prof. Z. L. Wang, Dr. Z. Kang[+]
School of Materials Science and Engineering
Georgia Institute of Technology
Atlanta, GA 30332-0245 (USA)
E-mail: zhong.wang@mse.gatech.edu
[+] Present address: Research Center for Functional Rare Earth Higher Oxides, Institute of Geomechanics, Beijing 100081, China.

  0935-9648/03/0603-0521 $ 17.50+.50/0